Environmental Science Nano

ROYAL SOCIETY OF CHEMISTRY

PAPER

View Article Online
View Journal

Cite this: DOI: 10.1039/d1en00185j

Effects of rhamnolipid biosurfactant on the dissolution and transport of silver nanoparticles in porous media†

Shuchi Liao,[a] Chen Liu,[a] Dorothea Pinchbeck,[a] Natalie L. Cápiro,[b] John D. Fortner,[c] Linda M. Abriola[a] and Kurt D. Pennell *[a]

Received 24th February 2021,
Accepted 14th July 2021

DOI: 10.1039/d1en00185j

rsc.li/es-nano

The effects of nanoscale silver (nAg) particles on subsurface microbial communities can be influenced by the presence of biosurfactants, which have been shown to alter nanoparticle surface properties. Batch and column studies were conducted to investigate the influence of rhamnolipid biosurfactant (1–50 mg L^{-1}) on the stability and mobility of silver nanoparticles (16 ± 4 nm) in batch reactors and water-saturated columns with three solution chemistries: pH = 4 and dissolved oxygen concentration (DO) = 8.8 mg L^{-1}, pH = 7 and DO = 8.8 mg L^{-1}, pH = 7 and DO = 2.0 mg L^{-1}. In batch studies, the presence of rhamnolipid (2–50 mg L^{-1}) reduced nAg dissolution by 83.3–99.1% under all pH and DO conditions. Improved nAg stability was observed when rhamnolipid was present in batch reactors at pH = 7 ± 0.2, where the hydrodynamic diameter remained constant (~50 nm) relative to rhamnolipid-free controls (increased to >230 nm) in 48 hours. Column experiments conducted at pH 4.0 ± 0.2 demonstrated that co-injection of nAg with rhamnolipid (2, 5 and 50 mg L^{-1}) decreased Ag^+ breakthrough from ~22% of total applied mass in rhamnolipid-free columns to less than 8.1% in the presence of rhamnolipid and altered the shape of the nAg retention profile from a hyper-exponential to a uniform distribution. Column experiments performed at pH 7.0 ± 0.2 and DO levels of either ~2.0 or ~8.8 mg L^{-1} showed that co-injection of 5 mg L^{-1} and 50 mg L^{-1} rhamnolipid increased nAg mass breakthrough by 25–40% and ~80%, respectively, enhancements in nAg stability and mobility were attributed to rhamnolipid adsorption on nAg surfaces, which effectively slowed the oxidation and thus release of Ag^+, and adsorption of rhamnolipid on the porous medium, which competed for nAg attachment sites. These results indicate that the presence of rhamnolipid significantly influenced nAg dissolution and mobility under dynamic flow conditions. A mathematical model based on modified filtration theory (MFT) accurately reproduced nAg transport and retention behavior when aggregation and reaction processes were minimal and when rhamnolipid was present, providing a tool to predict the effects of biosurfactants on nAg transport in porous media.

Environmental significance

Biological processes, including biotransformation, biofilm formation, and biosurfactant production, can substantially alter the fate of nanoparticles in the environment. While many studies have addressed the effects of biofilms on nanoparticle transport and retention, very few studies have investigated the influence of biosurfactants on nanoparticle behavior in porous media under dynamic conditions. In this study, the effect of rhamnolipid biosurfactant on the oxidative dissolution and transport of silver nanoparticles (nAg) was evaluated using a combination of batch and column experiments conducted at three environmental relevant conditions (pH = 4 or 7, DO = 2.0 or 8.8 mg L^{-1}). Batch studies showed that rhamnolipid reduced nAg dissolution under all pH and DO conditions, and that the presence of high concentration rhamnolipid (50 mg L^{-1}) improved nAg stability. Column studies revealed that rhamnolipid strongly reduced nAg dissolution under dynamic flow conditions and significantly enhanced nAg mobility through a combination of improved particle stability and competitive blocking of particle attachment sites. These findings demonstrate that biosurfactant can have a marked impact on nAg dissolution, transport and retention behavior in terrestrial systems, and could reduce the effects of nAg on microbial communities.

[a] School of Engineering, Brown University, 184 Hope Street, Box D, Providence, Rhode Island 02912, USA. E-mail: kurt_pennell@brown.edu
[b] Department of Civil and Environmental Engineering, Auburn University, Auburn, Alabama, 36849, USA
[c] Department of Chemical and Environmental Engineering, Yale University, New Haven, CT, 06520, USA

† Electronic supplementary information (ESI) available. See DOI: 10.1039/d1en00185j

Introduction

The production, use, and disposal of engineered nanomaterials (ENMs) have raised concerns over potential risks that ENMs pose to the environment and human health.[1] Understanding the fate of ENM in water and soil systems, likely major sinks for ENMs, is critical to exposure

control, risk assessment and regulatory policy.[2–4] Silver nanoparticles (nAg) are one of the most widely applied ENMs with a wide range of applications due to their broad antimicrobial properties.[5] However, release of nAg to the environment may impact ecosystems as a number of studies have shown that Ag^+ originating from nAg can exert deleterious effects on bacteria and aquatic organisms.[6–8] The oxidative dissolution of nAg depends on solution chemistry including pH, dissolved oxygen, and the presence of salts and/or dissolved organic carbon, as well as nAg properties such as size, shape, and surface functionalization.[9–12] To increase nAg stability and minimize dissolution during storage, nAg is commonly coated with a layer of organic molecules such as citric acid or polymer (*e.g.*, polyvinyl pyrrolidone).[13,14] However, even surface-coated nAg can still exhibit dissolution upon release to the environment.[15,16] To evaluate nAg dissolution process in the environment and its potential impact on microbial community, many studies have performed batch experiments using environmentally and/or biologically relevant solutions.[17–21] For instance, Mitrano *et al.* conducted nAg dissolution studies in batch reactors containing laboratory, natural and processed waters.[19] Yi *et al.* exposed nAg with cysteine and bovine serum albumin for 3–12 hours in batch reactors and monitored nAg dissolution and biotoxicity to a white-rot fungus.[21] However, most of these studies focused on batch reactor experiments, and did not account for nAg dissolution under flowing conditions. In fact, few studies have conducted column experiments to investigate nAg dissolution behavior in porous media under dynamic flow conditions. Thus, it is important to accurately account for nAg dissolution behavior when evaluating nAg transport and redistribution in environmental systems subject to water flow. Recent studies have demonstrated that the transport and deposition behavior of nAg is strongly influenced by co-existing constituents such as natural organic matter, polymers, surfactants, and colloids.[22–26] For instance, Park *et al.*[22] found that the deposition kinetics of sodium dodecyl sulfate (SDS) coated nAg were sensitive to humic acid (HA) concentrations. The mobility of nAg increased significantly with an increase of HA in the suspension. However, these studies mainly focused on the influence of co-existing constituents on nAg transport and retention processes, and very few studies have explored the simultaneous effects of co-constituents on nAg reactivity (*e.g.*, oxidative dissolution) and mobility in porous media under dynamic conditions.

Biological processes, such as biofilm formation, biodegradation, and biosurfactant production, can markedly affect the reactivity and mobility of nanoparticles in the subsurface. For example, biofilms can alter surface heterogeneity and pore structure of porous media, thus, enhancing nanoparticle retention.[27,28] Biodegradation of iron oxide nanocubes by bacteria can result in deformed particles and iron release.[29] Interestingly, the effects of microbially-produced biosurfactants on the subsurface stability and mobility of nanoparticles have received little attention, although several studies have concluded that biosurfactants can significantly change the surface properties of nanoparticles.[30]

Biosurfactants are defined as amphiphilic surface-active compounds produced and often excreted by microorganisms. Their low toxicity and biodegradability make them more environmentally friendly than many anthropogenic analogs, and thus, they have a number of applications in food, agriculture, medicine, and environmental remediation.[31,32] Rhamnolipid, a common biosurfactant, is generated by a variety of *Pseudomonas* species under a range of conditions (*e.g.*, pH 4–10).[33] It is also one of the most widely applied biosurfactants due to its high effectiveness in surface/interfacial tension reduction and commercial availability.[34] Furthermore, rhamnolipids have been integrated into nanotechnology, primarily for use as a surface modifier during nanoparticle synthesis.[28,35–39] Rhamnolipid-coated nanoparticles exhibit noticeable improvement in stability against agglomeration and deposition. For example, Marangon *et al.* found that the addition of rhamnolipid during nanoparticle synthesis reduced the size and polydispersity index of nanoparticles, and that rhamnolipid-stabilized nanoparticles exhibited a more positive surface charge with improved stability.[40] Basnet *et al.* reported that rhamnolipid coated iron nanoparticles exhibited superior colloidal stability and higher transport potential in saturated porous media compared to carboxymethyl cellulose and soy protein coated particles.[39] While numerous studies have utilized biosurfactants as a nanoparticle surface modifier,[41,42] little work has been done to evaluate the aggregation, reaction, and retention properties of nanoparticles in the presence of such biosurfactants. In prior work, we have investigated the effect of rhamnolipid on the transport and retention behavior of oleic-acid coated iron oxide nanoparticles in water-saturated columns packed with 80–100 mesh Ottawa sand. The presence of Rhamnolipid significantly enhanced nanoparticle mobility, through improved nanoparticle stability and by blocking attachment sites on the surfaces of quartz sand.[43] Since rhamnolipid could potentially alter nanoparticle surface properties and alter nanoparticle reactivity and mobility, it is possible that microorganisms in the subsurface that generate rhamnolipid will influence nAg dissolution and transport, and consequently, affect nAg bioavailability and antimicrobial properties. However, most studies have focused on the effects of biofilm on nAg transport and retention, while far less attention has been directed toward the potential impact microbial biosurfactants, such as rhamnolipid could have on nAg behavior in subsurface environments.

Thus, the goal of this work was to investigate the dissolution and transport behavior of nAg in the presence of rhamnolipid biosurfactant. To understand the influence of solution chemistry on nAg dissolution and Ag^+ release,[12,44] the effects of rhamnolipid on the aggregation, dissolution, and deposition behavior of nAg were evaluated as a function of pH (4 or 7), dissolved oxygen (DO) (2 or 8.8 mg L^{-1}), and rhamnolipid concentration (0,1, 2, 5, 50 mg L^{-1}). Batch experiments were conducted to evaluate the effects of

rhamnolipid on nAg aggregation and dissolution kinetics in batch reactors, while column experiments were performed to simultaneously assess the transport, deposition and dissolution behavior of nAg in a water-saturated quartz sand (80–100 mesh Ottawa sand) under dynamic flow conditions. Column effluent samples were collected continuously to construct breakthrough curves for total silver (TAg), nAg and Ag^+, and the columns were destructively sampled at the conclusion of each experiment to construct TAg retention profiles. To further interpret the experimental results, clean-bed filtration (CFT)[45] and modified filtration (MFT) models[46] were fit the effluent concentration and retention profile data to obtain nAg transport and retention parameters.

Material and methods

Materials

Citrate-coated silver nanoparticles (nAg) were synthesized using sodium borohydride as a reducing agent, sodium citrate as a stabilizer and silver nitrate as a precursor.[12,44] Briefly, a solution containing 0.4 mM trisodium citrate (Alfa Aesar, anhydrous, 99%) and 4 mM sodium borohydride (Millipore Sigma, >98%) was prepared in ice-cold (0 °C) deionized (DI) water (ELGA Purelab flex 4, 18.2 mΩ cm). A 15 mM $AgNO_3$ (Alfa Aesar, >99.9%) solution was added drop wise using a syringe pump (Fusion 101, Chemyx) at a flow rate of 0.7 mL min^{-1} under continuous stirring (700 rpm). After $AgNO_3$ addition, the stirring rate was reduced to 60 rpm and the resulting suspension was stirred overnight. The reaction byproducts were removed by three cycles of a DI water wash and ultrafiltration (Amicon Ultra Centrifugal Filters, 30 kDa, Millipore Sigma). This sodium borohydride reduction method produced ~80 mg L^{-1} citrate-coated nAg with a mean diameter of 16 ± 4 nm and a zeta potential of −40 ± 5 mV containing trace level silver ions (0.09 ± 0.01 mg L^{-1}). Prior to batch and column experiments, the nAg stock was diluted to 2.5–3 mg L^{-1}, consistent with concentrations used in previous studies.[10,21] Rhamnolipid biosurfactant (90% purity) was purchased from AGAE Technologies. The ratio of mono-rhamnolipid to di-rhamnolipid in this product is ~3 : 2, with a molecular weight of 563 g mol^{-1}. Rhamnolipid concentrations used in this work were 1, 2, 5, 10, 50 mg L^{-1}, which are in the range reported by a study that bacteria could potentially produce in the subsurface.[47] The 80–100 mesh size fraction of Ottawa sand (mean diameter (d_{50}) of 165 μm) was obtained from F65 sand (US Silica) and separated using a programmable sieve shaker (Tyler Ro-Tap, W.S. Tyler Industrial Group). Prior to use, the 80–100 mesh size fraction was cleaned using a sequential acid wash, water rinse, ultrasonication, and oven-drying procedure.[46] A clean quartz sand was selected for use to minimize confounding factors such as soil organic matter and allow for direct assessment of interactions between rhamnolipid and nAg.

Batch experiments

Batch experiments were conducted to investigate the aggregation and Ag^+ release kinetics of nAg in aqueous suspension as a function of rhamnolipid concentration under three solution chemistries: 1) pH = 4.0 ± 0.2 and DO = 8.8 ± 0.2 mg L^{-1}; 2) pH = 7.0 ± 0.2 and DO = 8.8 ± 0.2 mg L^{-1}; 3) pH = 7.0 ± 0.2 and DO = 2.0 ± 0.2 mg L^{-1}. The batch reactors consisted of 120 mL glass vials (Fisherbrand) containing 100 mL nAg aqueous suspension (initial concentration 2.5–3 mg L^{-1}) and wrapped with aluminum foil. The nAg aqueous suspensions were prepared in the following sequence: electrolyte solution preparation (10 mM $NaNO_3$), DO adjustment, pH adjustment, rhamnolipid addition and nAg addition. The addition of rhamnolipid and nAg resulted in minimal changes in the solution pH and DO. The DO concentration of 8.8 ± 0.2 mg L^{-1} was achieved by equilibration with air for at least 6 hours, while the DO level of 2.0 ± 0.2 mg L^{-1} was obtained by purging the solution with pure nitrogen (ultra-pure, Air Gas) for ~5 minutes. Sealed glove bags (X-37-37 glove bag, I2R) with 2.0 mg L^{-1} oxygen atmosphere were then used to conduct the remaining solution preparation procedures and to maintain the low DO level in the reactors. The DO levels in all batch reactors were monitored during each experiment, and the DO concentrations were relatively constant (±0.2 mg L^{-1}) since the reactors were in contact with air or 2.0 mg L^{-1} oxygen atmosphere. The batch reactors were sampled every 30 minutes in the first 3 hours, and then sampled at 6, 10, 20, 32, and 48 hours. Dissolved silver ions were separated from the solution using an ultrafiltration unit (Amicon Ultra Centrifugal Filters, 3 kDa, Millipore Sigma) for 20 minutes at 4200 rpm (Centrifuge 5804R, Eppendorf). Additionally, short-term aggregation kinetics of nAg were also monitored in 2 mL batch reactors (plastic cuvettes, Fisherbrand) using a continuous time-resolved dynamic scatter light (DLS) technique at 1 minute intervals (Zetasizer Nano ZS90, Malvern Analytical).

Column experiments

A total of 16 column experiments were conducted using the same three different solution chemistries used in the batch studies to assess the effect of rhamnolipid on the transport, retention, and reactivity of nAg in 80–100 mesh Ottawa sand (Table 1). The columns were packed with sand and completely saturated with water following procedures described by Wang *et al.*[46] Briefly, a borosilicate glass column (2.5 cm diameter × 15 cm length) was packed with washed 80–100 mesh Ottawa sand under vibration and flushed with CO_2 gas for at least 60 min to facilitate dissolution of entrapped gas during the water saturation process. At least 10 pore volumes (PVs) of background solution (10 mM $NaNO_3$) at the desired pH and DO level were introduced into the column in an up-flow mode using a high-performance liquid chromatography (HPLC) pump (ChromTech). After column saturation, a non-reactive tracer test was conducted, using a pH and DO concentration adjusted 10 mM NaBr solution, to characterize water flow and hydrodynamic dispersion. The effluent bromide ion concentrations were

Table 1 Summary of column experiments performed

Experimental conditions and results									Modeling results		
Column identifier[a]	Ag conc.[b] (mg L^{-1})	Rham. conc.[c] (mg L^{-1})	nAg size[d] (nm)	nAg Z.P.[e] (mV)	nAg B.T.[f] (%)	Ag^+ B.T.[g] (%)	Ag R.T.[h] (%)	M.B.[i] (%)	k_{att}[j] (h^{-1})	S_{max}[k] (μg g^{-1})	α[l]
pH4DO9R0(dup)	2.6 (2.8)[m]	0	24.8/32.1 (22.1/15.8)	−27.4/−27.6 (−23.0/−29.1)	0.9 (1.5)	22.0 (21.4)	79.8 (78.4)	102.8 (101.3)	NA[n]	NA	NA
pH4DO9R2	2.3	2	61.03/490.9	−26.2/−27.6	0.2	8.1	89.0	97.3	NA	NA	NA
pH4DO9R5(dup)	2.6 (2.5)	5	54.1/147.8 (43.3/110.6)	−18.4/−21.4 (−20.9/−19.5)	0.4 (1.0)	2.0 (3.6)	91.9 (89.9)	94.3 (94.5)	12.0 ± 2.8 (27.9 ± 0.4)	NA (NA)	0.03 (0.07)
PH4DO9R50	2.5	50	55.3/55.9	−26.4/−27.6	0.3	4.9	93.7	98.9	25.1 ± 12.5	2.2 ± 0.1	0.06
PH4DO9R2F	2.8	2 (flush)	NA	NA	0.3	8.1	98.2	106.6	NA	NA	NA
PH4DO9R5F	2.5	5 (flush)	NA	NA	0.6	10.0	80.4	91.0	NA	NA	NA
PH7DO9R0(dup)	2.6 (2.6)	0	41.1/71.8 (49.3/67.6)	−38.8/−38.5 (−35.5/−37.4)	2.9 (12.1)	4.5 (2.2)	99.8 (84.1)	107.3 (98.4)	14.6 ± 2.7 (11.0 ± 2.7)	2.5 ± 0.2 (2.3 ± 0.2)	0.04 (0.03)
PH7DO9R5	2.6	5	37.2/38.1	−38.4/−38.5	49.0	0.7	57.2	106.8	23.0 ± 14.2	1.1 ± 0.1	0.06
PH7DO9R50(dup)	2.9 (2.3)	50	39.0/37.1 (43.2/37.5)	−39.0/−37.1 (−43.2/−37.5)	87.4 (86.5)	2.9 (6.5)	19.3 (17.0)	109.7 (110.0)	13.2 ± 11.4 (2.5 ± 1.7)	0.4 ± 0.1 (0.2 ± 0.1)	0.03 0.01
PH7DOR0(dup)	2.9 (2.4)	0	40.7/43.9 (58.9/73.9)	−33.5/−34.6 (−37.4/−34.8)	29.2 (20.2)	1.0 (3.1)	69.1 (74.2)	99.3 (97.6)	7.0 ± 2.2 (9.1 ± 4.4)	1.7 ± 0.2 (1.5 ± 0.2)	0.02 (0.02)
PH7DOR5	2.6	5	40.6/33.1	−30.8/−32.8	44.7	2.4	49.6	96.7	6.1 ± 1.2	1.1 ± 0.1	0.02

[a] Column identifier: *R* represents rhamnolipid concentration (mg L^{-1}); (dup) stands for duplicate columns. [b] Total silver concentration in influent solution. [c] Rhamnolipid concentration in influent solution. [d] nAg hydrodynamic size at the start/end of injection. [e] nAg surface zeta potential at the start/end of injection. [f] % of nAg breakthrough. [g] % of silver ion (Ag^+) breakthrough. [h] % of retained nAg. [i] Mass balance. [j] First-order attachment rate of nAg. [k] Maximum retention capacity of nAg on sands. [l] Attachment efficiency.[45,53] [m] Replicate column data are shown in parenthesis. [n] NA: not applicable.

measured using an ion-selective electrode (Cole-Parmer) and fit to a one-dimensional form of the advective–dispersive–reactive (ADR) transport equation using CXTFIT ver 2.163 (ref. 48) to obtain the hydrodynamic dispersion coefficient (D_H) and retardation factor (R_F), as shown in Fig. S1.† Following the non-reactive tracer test, nAg influent solutions (2.5 mg L^{-1}) with different concentrations of rhamnolipid (0, 2, 5 or 50 mg L^{-1}) were prepared using the same procedure described in the batch experiments. Freshly prepared nAg influent solutions (3 PVs) were then injected to the column using a syringe pump (Fusion 101, Chemyx), followed by at least 9 PVs of background solution to evaluate the re-entrainment and release of Ag^+ from deposited silver nanoparticles. Column effluent samples were collected continuously using a fraction collector (CF-2, Spectrum Laboratories) and analyzed for total silver (TAg) concentration. Silver nanoparticles (nAg) were removed from effluent samples using 3 kDa Amicon ultrafiltration filters with centrifugation at 4200 rpm for 15 minutes. To avoid nAg dissolution in collection vials, each effluent sample was centrifuged immediately after collection to separate the Ag^+ from the nanoparticles. The eluent was analyzed for Ag^+, and the concentration of nAg was obtained by subtracting the Ag^+ concentration from the TAg concentration. To construct the effluent breakthrough curves, TAg and nAg concentrations were expressed as relative concentrations (C/C_0), where C_0 is the total influent silver concentration, and plotted *versus* the cumulative number of dimensionless pore volumes delivered to the column. To construct TAg retention profiles, the columns were sectioned into ten increments at the conclusion of each experiment and the solid-phase samples were digested in 15% nitric acid using a microwave digestion system (MARS 6, CEM Corp.). For column experiments performed at the lower DO level (2.0 mg L^{-1}), the entire process, including column saturation, tracer test, suspension preparation and effluent sample collection, was conducted in a glove bag with a 2 mg L^{-1} oxygen atmosphere.

In addition to column experiments described above, another two columns were performed at pH = 4.0 ± 0.2 and DO = 8.8 ± 0.2 mg L^{-1} to explore the effect of rhamnolipid solution on the reactivity of retained nAg. Here, following the introduction of 3 PVs of nAg-only solution, 3 PVs of nAg-free background solution were injected to displace any free particles, then 3 PVs of 2 mg L^{-1} or 5 mg L^{-1} rhamnolipid solution flush were applied, followed by another flush of 4–5 PVs background solution. All the column experiments were conducted at a constant flow rate of 1 ± 0.1 mL min^{-1}, which corresponds to a pore-water velocity of ~8.6 m per day. Duplicate experiments were conducted for 50% of the columns to confirm reproducibility. Experimental conditions and results for all column studies are summarized in Table 1.

Analytical methods

The hydrodynamic size and electrophoretic mobility of nAg suspension were characterized with a Malvern ZetaSizer Nano ZS90 device using dynamic light scattering (DLS) and laser Doppler velocimetry, respectively. The electrophoretic mobility was related to zeta potential using the Smoluchowski approximation.[49] All DLS and zeta potential measurements were conducted in triplicate at room temperature (22 ± 1 °C). Ultraviolet-visible (UV-vis) light spectra of nAg suspensions with different concentrations of rhamnolipid were also monitored with a Jasco V-730 UV-vis

spectrophotometer (Easton) to evaluate the changes in nAg size and surface chemistry. The absorbance spectra were recorded in a range from 300 nm to 700 nm.

Sand grains collected before and after nAg deposition in columns were imaged using an ultra-high-resolution field emitter scanning electron microscope (SEM) (Zeiss LEO 1530 VP), equipped with an energy dispersive spectrometer (EDS). Prior to SEM imaging and EDS analysis, air-dried sand grain samples were attached to carbon conductive tapes and coated with a layer of gold to increase the signal-to-noise ratio. nAg core size and morphology in different solution chemistries were captured using a field-emission transmission electron microscope (TEM, FEI Tecnai G2 Spirit) operated at 120 kV. To maintain the morphological characteristics of nAg, TEM samples were prepared by placing a carbon coated copper grid on top of a Kimwipe (Kimtech Science) and then depositing several drops (100 μL) of nAg suspension on the grid (Electron Microscopy Sciences). The water in nAg suspension was absorbed with Kimwipe immediately and the nAg was retained on the copper grid. Total silver content and Ag^+ concentration in aqueous samples and digested solid-phase samples were determined by inductively coupled plasma optical emission spectroscopy (ICP-OES, 7300 DV, Perkin Elmer). The solid-phase samples were digested in 15% HNO_3 (Fisher Chemical) using a microwave digestion system (MARS 6, CEM Corp.) at 190 °C for 15 min.[50] Seven-point calibration curves were constructed using silver nitrate solutions (10 μg L^{-1} to 2000 μg L^{-1}), which yielded linear fits with regression coefficients (R^2) of greater than 0.99. The detection limit of the ICP-OES methods for silver was 5 μg L^{-1}, estimated using a method reported by Armbruster *et al.*[51]

Mathematical modeling

When nAg aggregation and reactivity were negligible (*e.g.*, columns conducted at pH 7.0 ± 0.2 or in the presence of rhamnolipid biosurfactant), the transport and retention of nAg can be described using a mathematical model based on clean bed filtration theory (CFT).[45] Here, a one-dimensional mass balance equation that accounts for advection, dispersion, and solid-phase deposition can be written as:

$$\frac{\partial C}{\partial t} + \frac{\rho_b}{\theta_w}\frac{\partial S}{\partial t} = D_h\frac{\partial^2 C}{\partial x^2} - v_p\frac{\partial C}{\partial x} \quad (1)$$

$$\frac{\rho_b}{\theta_w}\frac{\partial S}{\partial t} = k_{att}C \quad (2)$$

where C and S are the nanoparticle aqueous and solid-phase concentration (M L^{-3} and M M^{-1}) respectively; t is time (t), x is the distance from the column inlet (L); v_p is the average pore-water velocity (L t^{-1}), D_h is the hydrodynamic dispersion coefficient for the column (L^2 t^{-1}), ρ_b is the bulk density of the porous medium (M L^{-3}), θ_w is the water content, and k_{att} is the first order attachment rate constant.

CFT predicts an exponential decay of retained particles with distance, however, some of our experimental retention profiles displayed nonmonotonic particle distribution, suggesting a limited or maximum retention capacity. Therefore, a modified filtration model (MFT)[52] was employed to simulate nAg transport and retention in these column experiments. Here, the eqn (2) is replaced by:

$$\frac{\rho_b}{\theta_w}\frac{\partial S}{\partial t} = k_{att}\frac{S_{max}-S}{S_{max}}C \quad (3)$$

where S_{max} is the maximum capacity of sand for nanoparticle deposition. As more nAg is retained on the solid phase (*i.e.*, increasing S), the effective attachment rate $k_{att}\frac{S_{max}-S}{S_{max}}$ decreases from 1 to 0.

The CFT and MFT models described by eqn (1)–(3) were implemented using a central-in-space and fully implicit-in-time finite difference scheme in MATLAB R2020a (The MathWorks). The nAg attachment rate constant (k_{att}) and maximum capacity (S_{max}) were estimated by fitting the model to experimental breakthrough curves and corresponding retention profiles using a least-squares optimization procedure in MATLAB with the following objective function:

$$f(x) = \alpha\frac{\sum_t(\mathrm{ExpBTC}-\mathrm{ModelBTC})^2}{\mathrm{Total\ Mass}} + \beta\frac{\sum_t(\mathrm{ExpRET}-\mathrm{ModelRET})^2}{\mathrm{Total\ Mass}} \quad (4)$$

Here, α and β are weighting factors equivalent to the fractions of total mass observed in the effluent and retained on the solid phase (*i.e.*, $\alpha + \beta = 1$), allowing the user to fit breakthrough (ExpBTC) and retention (ExpRET) data simultaneously.

Results and discussion

Effect of rhamnolipid on nAg dissolution kinetics

The results of batch reactor studies of nAg dissolution kinetics conducted as a function of rhamnolipid concentration (0, 1, 2, 5, 50 mg L^{-1}) under three environmentally relevant solution chemistries (pH = 4.0 ± 0.2 and DO = 8.8 ± 0.2 mg L^{-1}, pH = 7 ± 0.2 and DO = 8.8 ± 0.2 mg L^{-1}, and pH = 7.0 ± 0.2 and DO = 2.0 ± 0.2 mg L^{-1}) are shown in Fig. 1 and S2.† In the absence of rhamnolipid, citrate-coated nAg readily dissolved, releasing Ag^+ in acidic (pH = 4 ± 0.2) and oxygen-saturated (DO = 8.8 ± 0.2 mg L^{-1}) solutions over the course of 48 hours. However, when 2 mg L^{-1} rhamnolipid was present in the batch reactors, the extent of Ag^+ release decreased remarkably, from a maximum Ag^+ concentration of 0.9 mg L^{-1} to 0.35 mg L^{-1}. When higher concentrations of rhamnolipid (5 mg L^{-1} and 50 mg L^{-1}) were present, minimal amounts of Ag^+ were released (less than 0.02 mg L^{-1}). To quantify the effect of rhamnolipid concentration on the rate of Ag^+ release, a modified first-order kinetic model[54] was fit the batch experimental data. The model captured the results with R^2 greater than 0.89 for all experimental data and the fitted parameters were listed in Table S1.† At pH ~ 4 and DO ~ 9 mg L^{-1}, the fitted maximum dissolvable concentration of nAg decreased from 0.6526 mg L^{-1}

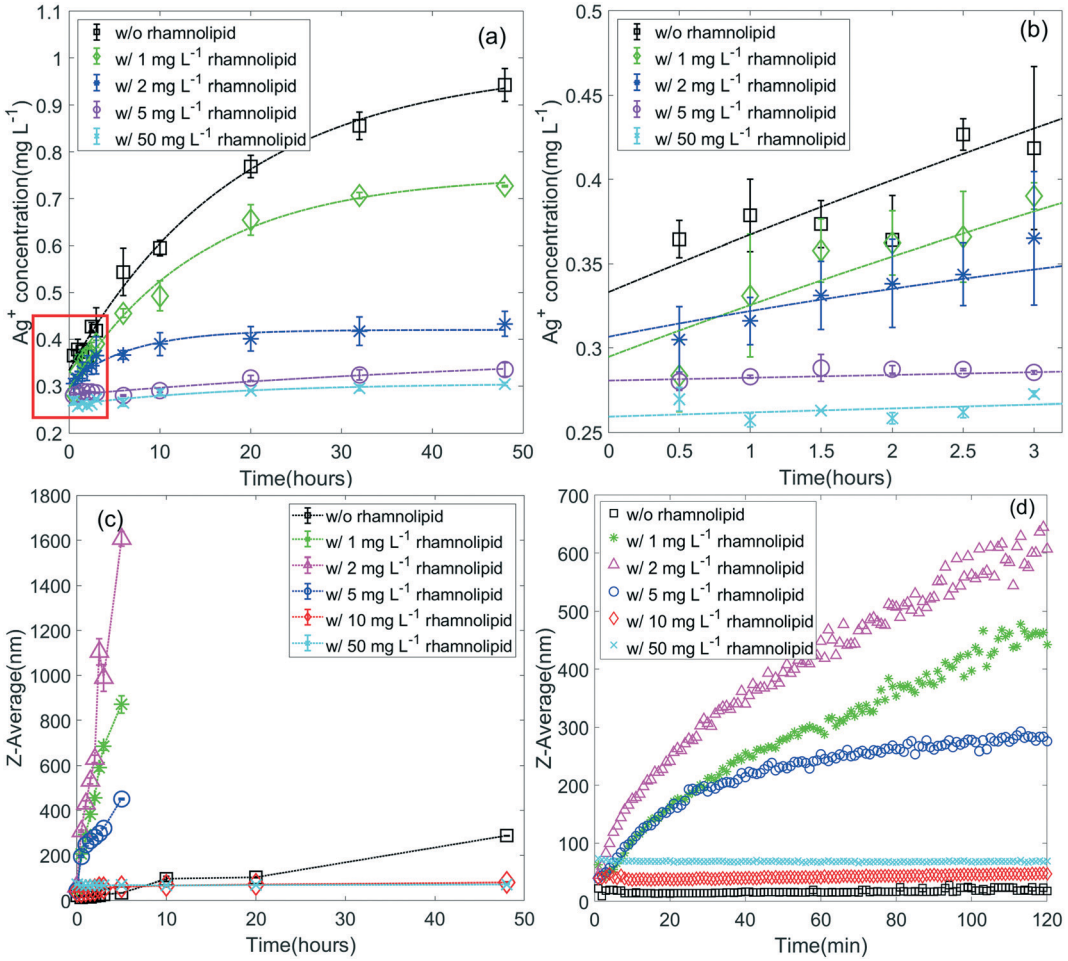

Fig. 1 (a and b) Ag^+ release kinetics at pH 4.0 ± 0.2 and dissolved oxygen concentration of 8.8 ± 0.2 mg L^{-1} in 48 hours, early time data (red box, first 3 hours) are enlarged in (b). (c and d) nAg aggregation kinetics at pH 4.0 ± 0.2 and dissolved oxygen concentration of 8.8 ± 0.2 mg L^{-1} in 48 hours (long term) and in 2 hours (short term). The Ag^+ release data were fit to a first order kinetics equation.[54] Error bar represents standard deviation of duplicate/triplicate measurements.

for rhamnolipid-free nAg suspension to 0.4553 mg L^{-1}, when 2 mg L^{-1} rhamnolipid was added, and further diminished by one order-of-magnitude (0.0467 mg L^{-1}) in the presence of 50 mg L^{-1} rhamnolipid.

These results suggest that less surface area of nAg was available for oxidation[54] due to adsorption of rhamnolipid. Similar results were obtained at pH 7 ± 0.2 and DO 8.8 ± 0.2 and pH 7 ± 0.2 and DO 2 ± 0.2 as shown in Fig. S2.† Observed inhibition of nAg dissolution is consistent with data reported by Dubas and Pimpan[55] who demonstrated that natural organic matter blocked oxidation sites on nAg and reduced the release of Ag^+. In our experiments, adsorption of rhamnolipid on nAg surfaces was confirmed by zeta potential measurement and UV-vis spectral data. As shown in Fig. S4,† under all pH and DO scenarios investigated, the zeta potential of nAg became less negative and the primary adsorption peak of nAg at ~400 nm shifted to higher wavelengths (red shift) when rhamnolipid was present, demonstrating that the surface charge was reduced and the amount of rhamnolipid on nanoparticle surfaces increased due to rhamnolipid adsorption,[9] respectively. Thus, the reduction in the release of Ag^+ can be attributed to rhamnolipid adsorption and a subsequent reduction in nAg oxidation/dissolution kinetics. An alternate explanation is that dissolved organic matter or rhamnolipid could act as antioxidants, scavenging reactive oxygen species and thereby preventing oxidative dissolution of nAg.[56] The antioxidant potential of rhamnolipid was examined in a recent study[57] and the results showed rhamnolipid only exhibited limited antioxidant activity, and was not comparable to a standard oxidant scavenger such as ascorbic acid.

Effect of rhamnolipid on nAg aggregation

The effect of rhamnolipid on nAg aggregation kinetics was evaluated as a function of both solution chemistry and rhamnolipid concentration. At pH 4.0 ± 0.2 and DO 8.8 ± 0.2, when no rhamnolipid was present, the mean nAg

hydrodynamic diameter decreased slightly at the beginning of the experiment and then remained relatively constant at 17 nm for the next 1.5 hours, followed by a steady increase to 300 nm at 48 hours (Fig. 1c and d). However, at the lower rhamnolipid concentrations (2 and 5 mg L^{-1}), nAg in the suspension agglomerated rapidly, with the average size increasing from ~22 nm to several hundred nanometers over 2 hours (Fig. 1c) and exceeding the measurement limit (~3 μm) in less than 10 hours (Fig. 1d). The resulting large size aggregates had reduced surface areas, which also contributed to decreased Ag^{+} release (Fig. 1a and b).[54,58] However, when the rhamnolipid concentrations in the batch reactors were 10 and 50 mg L^{-1}, the nAg suspension exhibited enhanced stability over 48 hours (50–60 nm). These observed aggregation and stabilization behaviors were consistent with measured changes of nAg zeta potential as a function of rhamnolipid concentration. As shown in Fig. S4a,† at the lower rhamnolipid concentrations (2 and 5 mg L^{-1}), the nAg zeta potential decreased with increasing rhamnolipid concentration, indicating rhamnolipid adsorption onto nAg surfaces, screening the nanoparticle surface charge. As a result, the electrostatic repulsion between nanoparticles decreased and agglomeration of nanoparticles increased. Additionally, nAg partially dissolved (Fig. 1a) and then aggregated (Fig. 2) at low rhamnolipid concentrations, which also contributed to the rapid aggregation of nAg. However, when rhamnolipid was subsequently increased to 50 mg L^{-1}, the negative charge was effectively restored as more anionic rhamnolipid was absorbed on nAg surfaces. The stabilization effect of higher concentration rhamnolipid therefore contributed to a greater negative surface charge and increased repulsive force between particles. Extended Derjaguin, Landau, Verwey and Overbeek (XDLVO) theory[59,60] was used to calculate interaction energies between nAg to support this mechanism. As shown in Fig. S7b,† the presence of 2 mg L^{-1} rhamnolipid resulted in a net attractive particle–particle energy profile for which no energy barrier was apparent. At higher rhamnolipid concentrations (50 mg L^{-1}), steric repulsive force created a stronger energy barrier between nanoparticles (>1000 kT). These XDLVO calculations are consistent with aggregation results and highlight the important role that steric forces play in nanoparticle stability when adsorbing polymers are present in solution. Similar to the results obtained at pH 4, when the pH was increased to 7 ± 0.2, the mean diameter of citrate-coated nAg gradually increased from 50 nm to ~95 nm over the 48 hours, and the addition of rhamnolipid (even at low concentration) improved nAg stability (Fig. S3†). Comparison of Fig. S3a and b and c and d,† reveals that DO concentration had a negligible effect on nAg aggregation kinetics. XDLVO calculations, plotted in Fig. S7c and d,† show that a large energy barrier exists when rhamnolipid is present in the nAg solution, thus, preventing nAg agglomeration.

To further assess the effects of rhamnolipid on nAg dissolution and aggregation, samples were imaged using TEM to evaluate changes in nAg size and morphology over time. Representative TEM images are shown in Fig. 2 and S5 and S6.† Fig. 2a, in which images were taken using samples at pH 4 ± 0.2 and DO of 8.8 ± 0.2 mg L^{-1} in the absence of rhamnolipid, illustrate the dissolution, deformation and aggregation processes of nAg in a rhamnolipid-free solution. After 20 hours, the initially spherical nAg was deformed into irregular shapes due to dissolution and/or aggregation. With 2 mg L^{-1} rhamnolipid in the nAg suspension (Fig. 2b), large

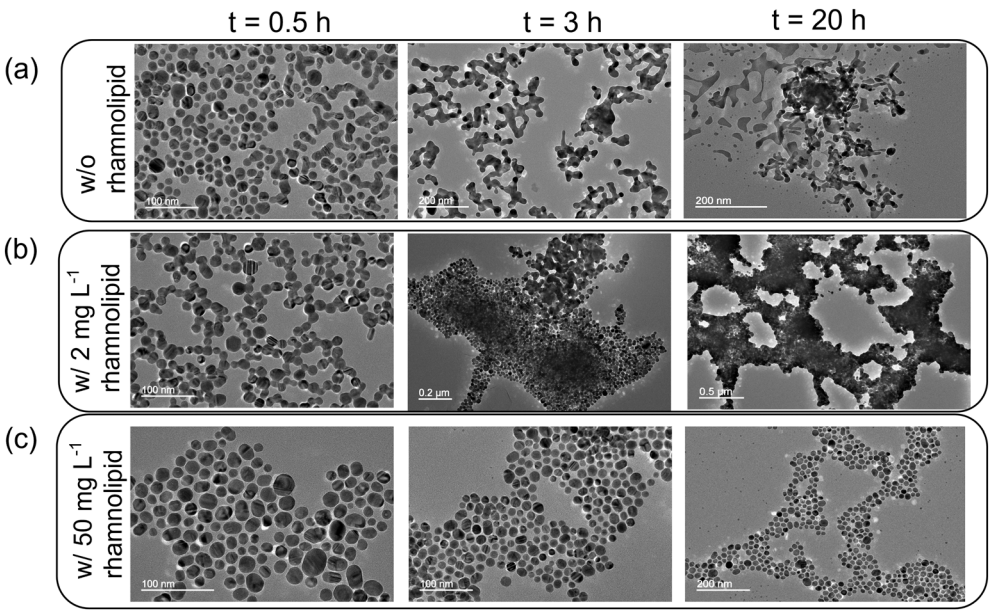

Fig. 2 Representative TEM images of nAg morphology changes over 20 hours (a) without rhamnolipid or (b) with 2 mg L^{-1} or (c) 50 mg L^{-1} rhamnolipid under a solution chemistry condition of pH 4.0 ± 0.2 and DO 8.8 ± 0.2 mg L^{-1}.

aggregates were formed, consistent with the DLS results discussed above. However, when 50 mg L^{-1} rhamnolipid was present, nAg size and morphology remained basically unchanged (Fig. 2c), demonstrating the stabilization effect of a higher concentration of rhamnolipid. At pH = 7 ± 0.2, observed changes in nAg morphology were negligible (Fig. S5 and S6†) in both rhamnolipid-free or 5 mg L^{-1} rhamnolipid samples, indicating that the nAg suspension was relatively stable at pH 7, even at a DO concentration of 8.8 mg L^{-1}.

Effects of rhamnolipid on nAg transport, retention and dissolution under acidic, oxic conditions

The total silver (TAg), nano silver (nAg) and silver ion (Ag^+) breakthrough curves and total silver retention profiles for column experiments conducted under an acidic and oxic condition (pH = 4 ± 0.2 and DO = 8.8 ± 0.2 mg L^{-1}) with different concentrations of rhamnolipid are presented in Fig. 3a–d, respectively. The hydrodynamic diameter and zeta potential of nAg in the influent suspension (~2.5 mg L^{-1} nAg with ~0.2 mg L^{-1} Ag^+) were monitored at the start and end of the injection period (3 PVs, ~1.5 hours). The presence of ~0.2 mg L^{-1} Ag^+ in the influent solution was assumed to have a negligible effect on nAg transport and retention processes based on prior experiments which showed that Ag^+ exhibits minimal adsorption on washed Ottawa sand at low concentrations.[44] A summary of column results, including the percent nAg and Ag^+ detected in the column effluent, nAg retained, and total mass balance, is shown in Table 1.

When nAg was introduced to the column without rhamnolipid, 22.9% of the total injected Ag mass was measured in effluent samples. The majority of silver mass eluted from the column in the form of Ag^+ with minimal breakthrough of nAg (0.9–1.5% of total mass). After injecting of 3 PVs of nAg suspension, 9 PVs of nAg-free background solution (pH = 4 ± 0.2 and DO = 8.8 ± 0.2) was flushed through the column to monitor dissolution of retained nAg. During this phase of the experiment, only minimal amounts (<0.5% of injected mass) of nAg were detected in effluent samples (Fig. 3b), consistent with previous studies that observed negligible detachment of nanoparticle when solution chemistries remain constant.[4] Retained nAg slowly dissolved during the background flush, resulting in a steady release of Ag^+ at a concentration of ~0.15 mg L^{-1} (Fig. 3c). The Ag^+ release concentration was several times greater than that measured in batch experiments (~0.02 mg L^{-1} dissolutions of nAg) during the same residence time (0.5 h). This observation was attributed to water flow in columns, which effectively removed dissolved Ag^+ from nAg surface and kept the surface constantly in contact with fresh solution containing O2/protons. This finding highlights the difference between nAg dissolution under batch reactors and dynamic flow conditions

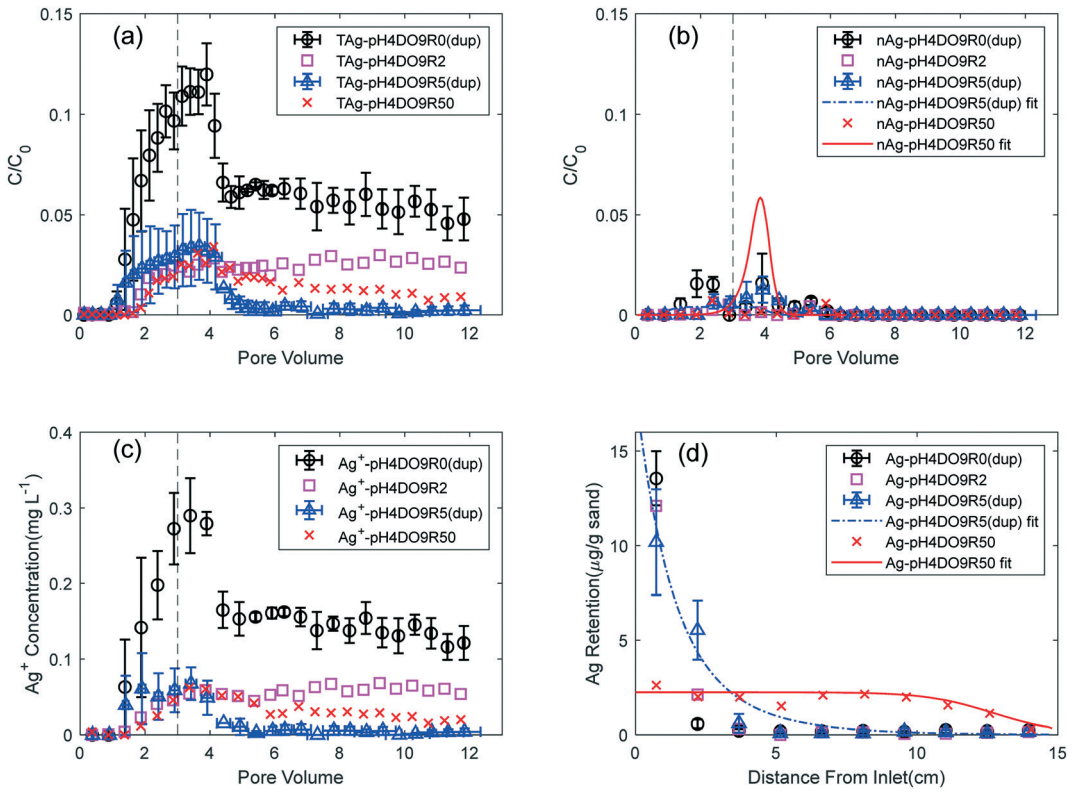

Fig. 3 Effect of rhamnolipid co-injection on Ag transport and elution under acidic pH/oxic conditions. (a) Experimental results for total silver (TAg) breakthrough, (b) experimental and modeling results for silver nanoparticle (nAg) breakthrough, (c) experimental resultsfor silver ion (Ag^+) breakthrough, and (d) experimental and modeling results for retained silver as a function of distance from column inlet for columns conducted at pH 4.0 ± 0.2 and DO 8.8 ± 0.2 mg L^{-1}.

and demonstrates the importance of performing nAg dissolution experiments under dynamic conditions.

The retention profiles of duplicate nAg columns exhibit hyper-exponential decay with highest solid phase concentrations measured near the column inlet (Fig. 3d). Similarly shaped retention profiles were reported for UV light aged nAg transport in porous media.[50] One possible explanation for this observation is that, when rhamnolipid was absent, dissolution significantly changed the nAg surface properties and increased its attachment efficiency near the column inlet. Since few research investigations have considered nanoparticle retention behavior under dissolution, the detailed mechanisms need further investigation. In the second set of column experiments, rhamnolipid was added to the influent nAg suspensions at environmentally relevant concentrations (2, 5, 50 mg L^{-1}) and co-injected with nAg. For the rhamnolipid concentration of 2 mg L^{-1}, TAg breakthrough concentration reached a maximum C/C_0 of ~0.025 and only 8.3% of the injected TAg mass eluted from the column. For rhamnolipid concentrations of 5 and 50 mg L^{-1}, even less TAg mass was measured in column effluents (3.1% and 5.2% of total applied mass, respectively) (Table 1 and Fig. 3a). Similar to rhamnolipid-free columns, most of the eluted TAg mass was detected as Ag^+ and nAg breakthrough was minimal (0.2–1% of total injected mass) for all rhamnolipid co-injection columns (Fig. 3b). Over the course of the 9 PV background solution flush, the concentration of dissolved Ag^+ in co-injection columns decreased by 66.7–96.8% compared to rhamnolipid-free columns, from 0.15 mg L^{-1} to 0.05 mg L^{-1} for 2 mg L^{-1} rhamnolipid and nearly to the detection limit (0.005 mg L^{-1}) for 5 and 50 mg L^{-1} rhamnolipid, respectively (Fig. 3c), consistent with the batch results that the addition of rhamnolipid resulted in reduced nAg dissolution, indicating that the presence of rhamnolipid influenced nAg dissolution under both batch reactor and dynamic flow conditions.

The nAg retention profiles for columns co-injected with 2 mg L^{-1} rhamnolipid displayed similar hyper-exponential decay with distance from the column inlet compared to nAg-alone columns (Fig. 3d). Over the course of the injection period (1.5 hours), the mean diameter of nAg in the influent increased substantially from 61 nm to 490.9 nm with 2 mg L^{-1} rhamnolipid (Table 1). Based upon a critical particle to grain ratio of 0.002 reported by Bradford

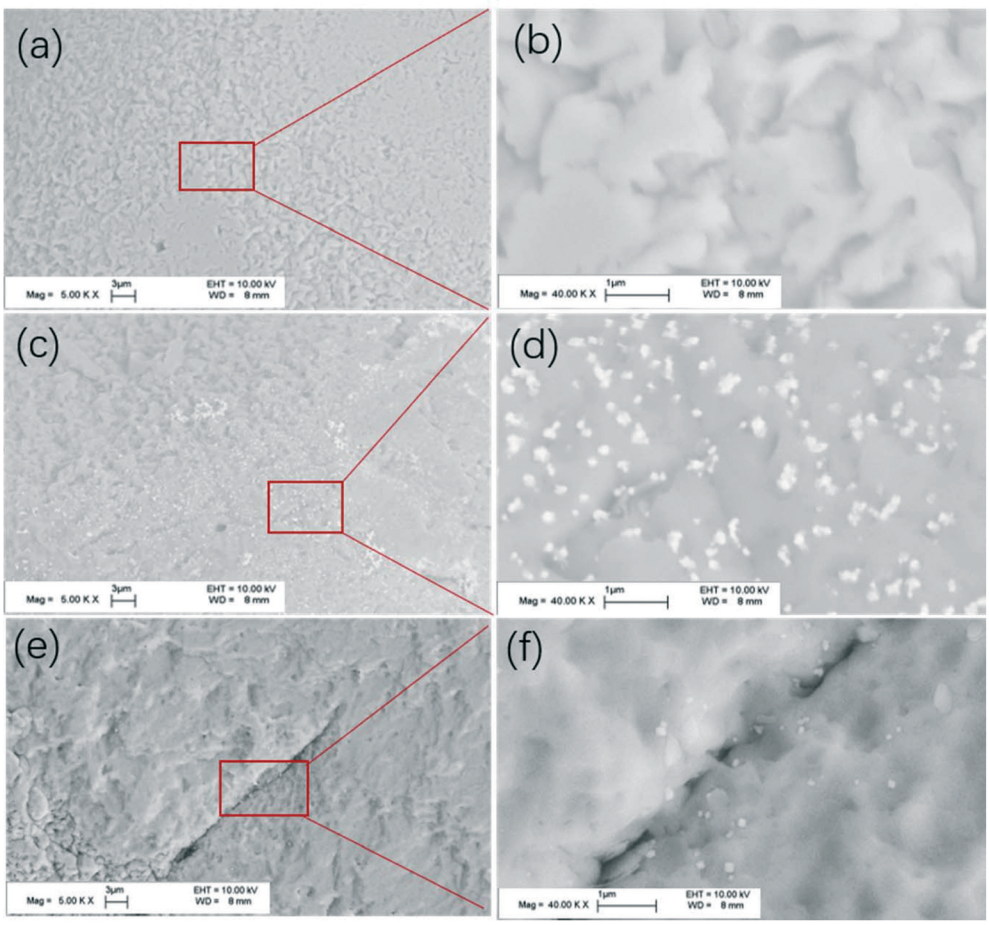

Fig. 4 Representative SEM images of (a and b) clean sand surface, (c and d) densly nAg/nAg aggregate deposited sand surface and (e and f) sparsely nAg deposited sand surface. Samples were collected from column inlets of PH4DO9R2 and PH7DO9R5 for (c and d) and (e and f), respectively.

et al.,[61] a nanoparticle size greater than 330 nm would be required to result in physical straining. Thus, the observed hyper-exponential nAg retention profile in 2 mg L^{-1} rhamnolipid column could be attributed to nAg aggregation and physical straining. SEM images of a sand grain collected from the inlet of 2 mg L^{-1} rhamnolipid co-injection column revealed that both nAg and nAg aggregates were deposited on sand surfaces and the density of particle deposition varied with the sand surface heterogeneity (Fig. 4c and d), further supporting the proposed aggregation, straining and attachment process for nAg deposition at low rhamnolipid concentrations. With 5 mg L^{-1} rhamnolipid in the influent suspension, retention of nAg exhibited an exponential decrease along the column length (Fig. 3d), consistent with predictions of CFT.[45] Retention profiles were fit to a CFT model (eqn (1) and (2)) to obtain the attachment efficiency (α) and rate constant (k_{att}). When 50 mg L^{-1} rhamnolipid was co-injected with nAg, a relatively flat retention profile was observed (Fig. 3d), with retained nAg concentration distributed uniformly along the column, indicating a limiting or maximum attachment capacity. This retention behavior is consistent with the observation reported by Wang *et al.*[62] that Fullerene (C60) nanoparticles were retained uniformly with distance when 20 mg C L^{-1} Suwannee river humic acid (SRHA) or fulvic acid (SRFA) were present in the suspension. The modified filtration model (MFT),[52] which accounts for nanoparticle maximum retention capacity (eqn (3)), was used to fit the column data. Model results indicate a retention capacity of 2.2 μg nAg per gram sand under this condition (50 mg L^{-1} rhamnolipid, pH 4 ± 0.2 and DO = 8.8 ± 0.2).

Effect of lower concentration rhamnolipid flush on the dissolution of retained nAg

To further explore the effect of rhamnolipid on the dissolution behavior of retained nAg, two additional column experiments were performed at pH 4 ± 0.2 and DO = 8.8 ± 0.2 mg L^{-1}. Here, 3 PVs of a ~2.5 mg L^{-1} nAg only influent suspension was injected to deposit nAg, followed by 3 PVs background to displace any unattached nAg. Then 3 PVs of a 2 or 5 mg L^{-1} rhamnolipid solution (pH 4 ± 0.2 and DO = 8.7 mg L^{-1}) was introduced to the column, followed by another 5 PVs rhamnolipid-free background solution. As shown in Fig. 5, Ag^+ concentration in the effluent started to decline after the injection of 1 PV of rhamnolipid solution (at ~7 PV), and Ag^+ levels remained very low (close to detection limit of 5 μg L^{-1}) even after the column was flushed with another 5 PVs background solution. As a result, compared to the rhamnolipid-free columns, much less Ag^+ was detected in effluent samples when the rhamnolipid flush was applied (12.2% *vs.* 2.8% of total injected Ag mass). The reduction in nAg dissolution after the rhamnolipid flush could be attributed to adsorption of rhamnolipid on deposited nAg, which acted to protect the nAg core from further oxidation and release of Ag^+. Combined with the results from the co-injection columns, these findings indicate that the presence of rhamnolipid (even at low concentrations) in the subsurface could significantly reduce dissolution of retained nAg even under relatively fast flow velocities.

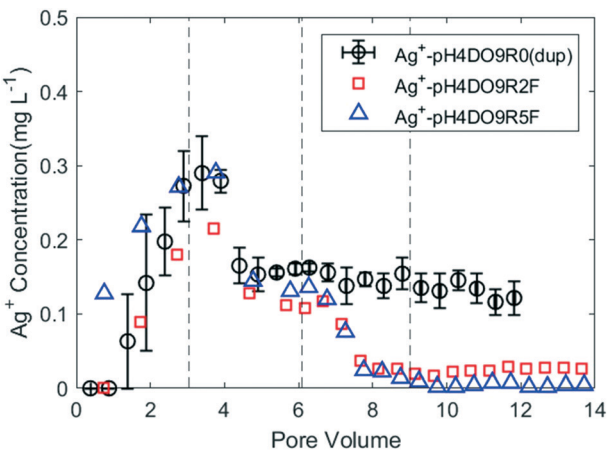

Fig. 5 Effect of rhamnolipid flush on retained Ag elution under acidic pH/oxic conditions. Experimental results of silver ion (Ag^+) breakthrough for columns conducted with pH 4.0 ± 0.2, DO 8.8 ± 0.2 mg L^{-1} and flushed with 2 mg L^{-1} or 5 mg L^{-1} rhamnolipid after silver nanoparticle deposition.

Effect of rhamnolipid on nAg transport, retention, and dissolution under neutral/oxic condition

Column experiments were also conducted under a neutral and oxic scenario (pH 7 ± 0.2 and DO = 8.8 ± 0.2) to further evaluate the impact of rhamnolipid on nAg dissolution and transport behavior. The experimental and mathematical results are summarized in Table 1 and presented in Fig. 6. In the absence of rhamnolipid, 7.4–14.3% of applied TAg mass was detected in the column effluent, with 2.2–4.5% eluting as Ag^+ (Table 1). The resulting nAg breakthrough curve (Fig. 6b) exhibited an asymmetrical shape, with the relative nAg concentration (C/C_0) gradually increasing to a maximum value of 0.2 and then rapidly declining to below the detection limit (5 μg L^{-1}). During the subsequent background (9 PVs rhamnolipid-free) flush the Ag^+ concentration in the effluent was ~0.02 mg L^{-1} (Fig. 6c) and the Ag^+ during the last 6 PV flush accounted for only 0.9–1.9% of the applied TAg, indicating that at circumneutral pH conditions, dissolution of retained nAg was limited, consistent with prior studies.[10,63] When 5 mg L^{-1} rhamnolipid was introduced to the nAg influent solution, breakthrough of TAg increased remarkably, to 49.7% of the injected Ag mass, with 98.6% associated with nAg (Table 1). The effluent breakthrough curve for this case reveals that nAg was detected at 2 PV and the relative concentration (C/C_0) rapidly increased to 1 and then declined back to 0 immediately after the pulse injection ceased (Fig. 6b). The Ag^+ effluent breakthrough curves were similar to those obtained in the absence of rhamnolipid (Fig. 6c), except that Ag^+ concentrations approached the detection limit during the background flush. When 50 mg L^{-1} rhamnolipid was co-injected with nAg, even more applied silver

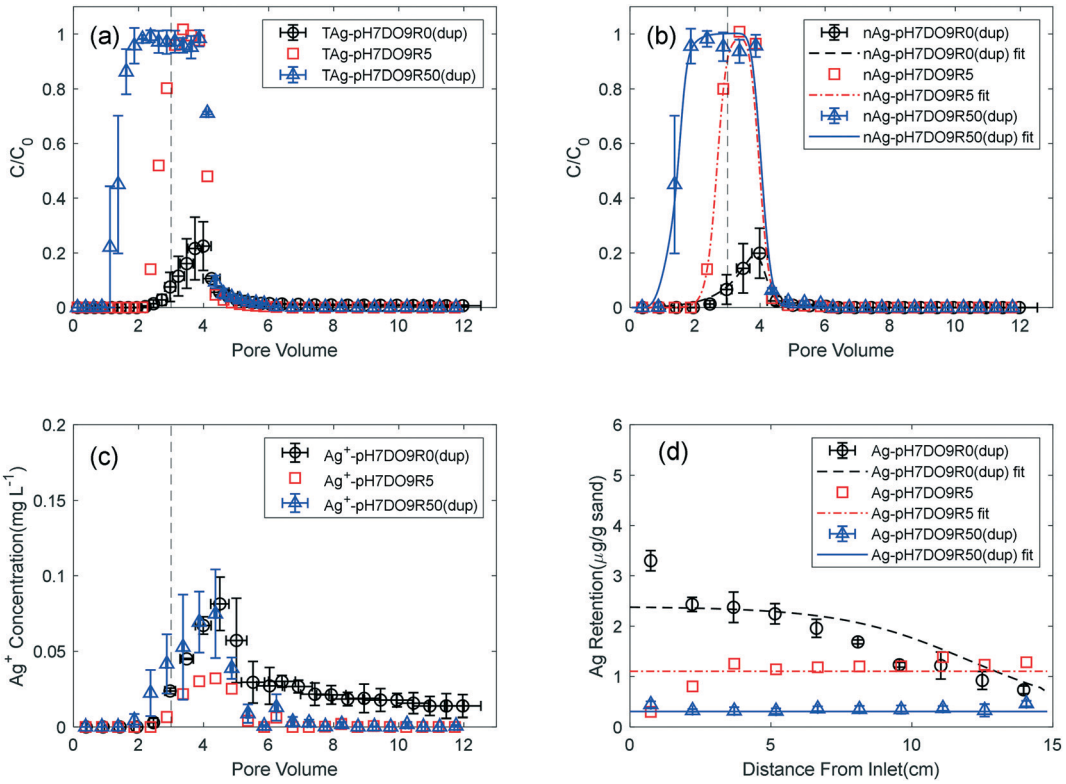

Fig. 6 Effect of rhamnolipid co-injection on Ag transport and elution under neutral pH/oxic conditions. (a) Experimental results of total silver (TAg) breakthrough, (b) experimental and modeling results of silver nanoparticle (nAg) breakthrough, (c) experimental results of silver ion (Ag^+) breakthrough, and (d) experimental and modeling results of retained silver as a function of distance from column inlet for columns conducted with pH 7.0 ± 0.2 and DO 8.8 ± 0.2 mg L^{-1}.

mass was measured in the column effluent (86.5–87.4%), and similarly, most of the TAg mass eluted from the column as nAg, with minimal dissolution (Fig. 6b and c). Our previous study of rhamnolipid adsorption on washed 80–100 mesh Ottawa sand indicated that rhamnolipid could be readily absorbed and occupy the adsorption/attachment sites on the sand surfaces.[43] Thus, the increased mobility of nAg in the presence of 5 mg L^{-1} and 50 mg L^{-1} rhamnolipid at pH 7 ± 0.2 and DO = 8.8 ± 0.2 mg L^{-1} was attributed to two factors: 1) adsorption of rhamnolipid on nAg increased the repulsive force between nAg and sand surfaces, as shown in XDLVO calculations (Fig. S8c†),[64,65] and 2) rhamnolipid was absorbed on sand surfaces and subsequently blocked potential attachment sites, the resulting retention profiles for all pH 7 and DO 8.8 columns were relatively uniform suggesting that nAg attachment exhibited a limiting or maximum capacity under these experimental conditions. SEM images showed that nAg was sparsely attached on the sand surface, with greater attachment to surface sites near the slit (Fig. S4e and f†), consistent with observations of other stabilized nanoparticle studies.[4] Due to the limited dissolution and constant nAg size, the MFT model (eqn (3)) was used to fit the nAg breakthrough curves and retention profiles. As shown in Fig. 6, the MFT model captured the general shape of both the breakthrough curves and retention profiles, with R^2 values of greater than 0.94. The model-fitted attachment parameters (Table 1) suggest the addition of rhamnolipid reduced the maximum capacity (S_{max}) of the sand for nAg deposition from 2.5 μg g^{-1} to 0.3 μg g^{-1} with only a slight decrease in attachment rates (*e.g.*, 14.6 h^{-1} and 13.2 h^{-1}).

Effect of rhamnolipid on nAg transport, retention and dissolution under neutral/hypoxic condition

Three column experiments were performed to understand the effects of rhamnolipid on nAg transport and retention under neutral and hypoxic conditions (pH = 7 ± 0.2 and DO = 2 ± 0.2 mg L^{-1}). The breakthrough of nAg in the absence of rhamnolipid ranged from 20.2 to 29.2% of applied nAg (by mass), which is greater than that observed in the neutral/oxic columns (2.9–12.1%) and consistent with data reported by Mittleman *et al.*[44] Similar to neutral/oxic columns, addition of 5 mg L^{-1} rhamnolipid increased nAg breakthrough from 20.2–29.2% to 44.7% of injected nAg mass, suggesting enhanced nAg mobility when rhamnolipid was present. The dissolution of retained nAg was minimal in both the rhamnolipid-free and 5 mg L^{-1} rhamnolipid columns (Fig. 7c). These nAg breakthrough curve and retention profile data were fit to MFT model, and the resulting attachment rate constants were smaller than those obtained under oxic conditions, consistent with a greater energy barrier between nAg and sand surfaces under these conditions (see XDLVO calculation in Fig. S8d†).

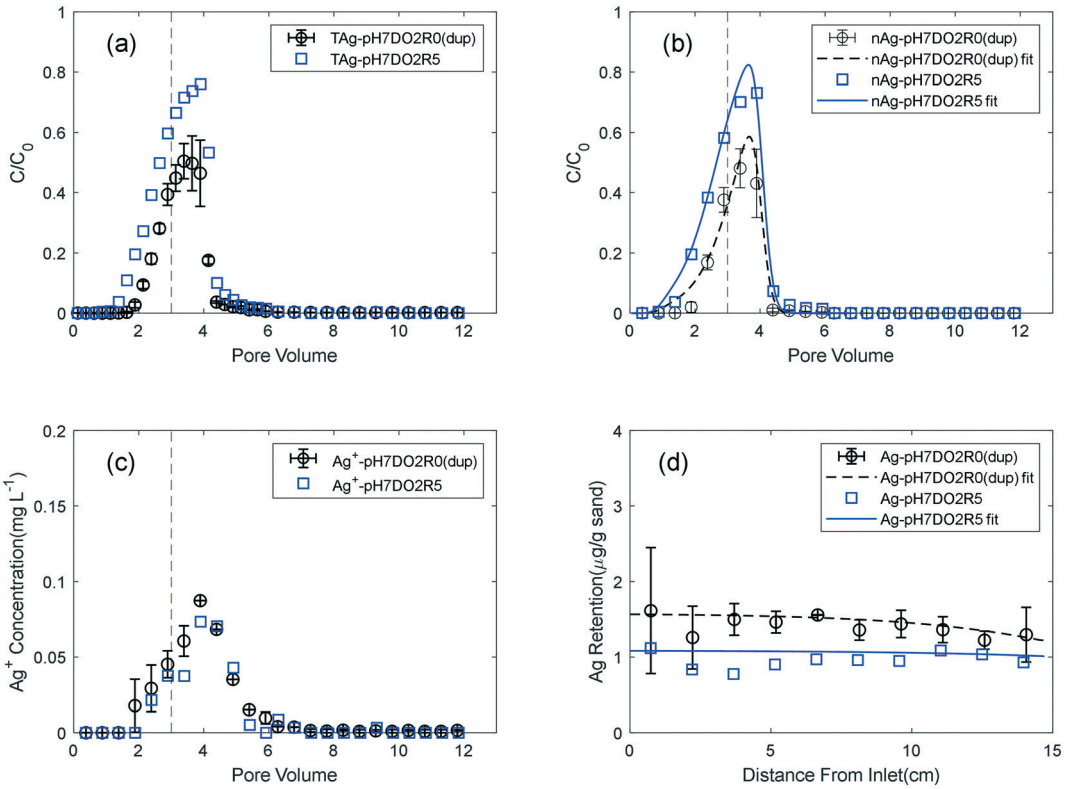

Fig. 7 Effect of rhamnolipid co-injection on Ag transport and elution under neutral pH/hypoxic conditions. (a) Experimental results of total silver (TAg) breakthrough, (b) experimental and modeling results of silver nanoparticle (nAg) breakthrough, (c) experimental results of silver ion (Ag^+) breakthrough, and (d) experimental and modeling results of retained silver as a function of distance from column inlet for columns conducted with pH 7.0 ± 0.2 and DO 2.0 ± 0.2 mg L^{-1}.

Conclusions

The effects of rhamnolipid biosurfactant on nAg aggregation, transport, and dissolution in batch and column systems were evaluated as a function of pH, DO and rhamnolipid concentration. Batch studies showed that the presence of rhamnolipid, even at low concentrations (2 and 5 mg L^{-1}), reduced nAg dissolution under all three pH and DO conditions. However, the effect of rhamnolipid on nAg aggregation was dependent upon both the rhamnolipid concentration and the pH of the solution; enhanced nAg stability was observed at pH 7 in the presence of rhamnolipid, while aggregation was detected for the pH = 4 and DO = 8.8 mg L^{-1} condition. Increasing the rhamnolipid concentration to 50 mg L^{-1} at pH 4 resulted in a stable nAg suspension. The behavior observed at higher concentration was attributed to adsorption of rhamnolipid on nAg, which slowed down the oxidation/dissolution process and increased the repulsive force between nanoparticles. Column experiments were then conducted at the three pH and DO conditions to investigate the effect of rhamnolipid on nAg transport, retention, and dissolution behavior under dynamic flow conditions. At pH 4 and DO = 8.8 mg L^{-1}, minimal nAg breakthrough was observed for both rhamnolipid-free and rhamnolipid-amended cases. However, the dissolved Ag^+ concentration detected in the column effluent decreased markedly in the presence of rhamnolipid. The corresponding nAg retention profiles also changed from hyper-exponential decay (0 or 2 mg L^{-1} rhamnolipid) to a uniform distribution with distance from the column inlet when the rhamnolipid concentration was increased to 50 mg L^{-1}, suggesting the stabilizing and attachment site blocking effects of rhamnolipid. Additionally, a 3PV flush of low concentration rhamnolipid (2 or 5 mg L^{-1}) greatly reduced the dissolution of retained nAg on sands, suggesting rhamnolipid preferentially absorbed to citrate-coated nAg and inhibited Ag^+ release. These findings indicate that the presence of rhamnolipid in porous media could significantly reduce the dissolution process of both free nAg and deposited nAg under dynamic flow conditions. At pH 7 and DO = 8.8 mg L^{-1}, the mass of eluted nAg increased with increasing rhamnolipid concentration, which was attributed to attachment site blocking by adsorbed rhamnolipid. Similar increases in nAg mobility in the presence of rhamnolipid were also observed at pH 7 and DO = 2 mg L^{-1}, suggesting rhamnolipid could also facilitate nAg transport process in porous media. A mathematical model based on modified filtration theory, which accounts for a maximum retention capacity, was able to accurately fit the column experimental data when nAg dissolution and aggregation were negligible. Fitted model parameters indicate that the presence of rhamnolipid resulted in a limiting or maximum retention capacity for nAg. These findings are relevant to subsurface environments where biosurfactant-producing bacteria are

ubiquitous and demonstrate that rhamnolipid can significantly alter both the mobility and reactivity of nAg in porous media, suggesting that bacteria can alter nAg bioavailability and antimicrobial property through biosurfactant production.

Conflicts of interest

There are no conflicts to declare.

Acknowledgements

Support for this research was provided by the National Science Foundation (NSF), award number CBET-1705346. The work has not been subject to NSF review, and therefore, does not necessarily reflect the views of the organization and no official endorsement should be inferred. Special thanks to The Institute for Molecular and Nanoscale Innovation (IMNI) at Brown University for use of their electronic imaging facility.

References

1 K. L. Garner and A. A. Keller, Emerging patterns for engineered nanomaterials in the environment: a review of fate and toxicity studies, *J. Nanopart. Res.*, 2014, **16**, 2503.
2 C. M. Park, K. H. Chu, J. Heo, N. Her, M. Jang, A. Son and Y. Yoon, Environmental behavior of engineered nanomaterials in porous media: a review, *J. Hazard. Mater.*, 2016, **309**, 133–150.
3 C. Ma, X. Huangfu, Q. He, J. Ma and R. Huang, Deposition of engineered nanoparticles (ENPs) on surfaces in aquatic systems: a review of interaction forces, experimental approaches, and influencing factors, *Environ. Sci. Pollut. Res.*, 2018, **25**, 33056–33081.
4 X. Meng and D. Yang, Critical Review of Stabilized Nanoparticle Transport in Porous Media, *J. Energy Resour. Technol.*, 2019, **141**, 070801.
5 C. Levard, E. M. Hotze, G. V. Lowry and G. E. Brown, Jr., Environmental transformations of silver nanoparticles: impact on stability and toxicity, *Environ. Sci. Technol.*, 2012, **46**, 6900–6914.
6 M. Akter, M. T. Sikder, M. M. Rahman, A. K. M. A. Ullah, K. F. B. Hossain, S. Banik, T. Hosokawa, T. Saito and M. Kurasaki, A systematic review on silver nanoparticles-induced cytotoxicity: Physicochemical properties and perspectives, *J. Adv. Res.*, 2018, **9**, 1–16.
7 C. Marambio-Jones and E. M. V. Hoek, A review of the antibacterial effects of silver nanomaterials and potential implications for human health and the environment, *J. Nanopart. Res.*, 2010, **12**, 1531–1551.
8 O. Choi, K. K. Deng, N. J. Kim, L. Ross, Jr., R. Y. Surampalli and Z. Hu, The inhibitory effects of silver nanoparticles, silver ions, and silver chloride colloids on microbial growth, *Water Res.*, 2008, **42**, 3066–3074.
9 I. L. Gunsolus, M. P. S. Mousavi, K. Hussein, P. Bühlmann and C. L. Haynes, Effects of Humic and Fulvic Acids on Silver Nanoparticle Stability, Dissolution, and Toxicity, *Environ. Sci. Technol.*, 2015, **49**, 8078–8086.
10 T. S. Peretyazhko, Q. Zhang and V. L. Colvin, Size-Controlled Dissolution of Silver Nanoparticles at Neutral and Acidic pH Conditions: Kinetics and Size Changes, *Environ. Sci. Technol.*, 2014, **48**, 11954–11961.
11 M. Tejamaya, I. Römer, R. C. Merrifield and J. R. Lead, Stability of Citrate, PVP, and PEG Coated Silver Nanoparticles in Ecotoxicology Media, *Environ. Sci. Technol.*, 2012, **46**, 7011–7017.
12 J. Liu and R. H. Hurt, Ion release kinetics and particle persistence in aqueous nano-silver colloids, *Environ. Sci. Technol.*, 2010, **44**, 2169–2175.
13 N. G. Bastús, F. Merkoçi, J. Piella and V. Puntes, Synthesis of Highly Monodisperse Citrate-Stabilized Silver Nanoparticles of up to 200 nm: Kinetic Control and Catalytic Properties, *Chem. Mater.*, 2014, **26**, 2836–2846.
14 L. Mulfinger, S. D. Solomon, M. Bahadory, A. V. Jeyarajasingam, S. A. Rutkowsky and C. Boritz, Synthesis and study of silver nanoparticles, *J. Chem. Educ.*, 2007, **84**, 322.
15 L. Gutierrez, C. Aubry, M. Cornejo and J.-P. Croue, Citrate-Coated Silver Nanoparticles Interactions with Effluent Organic Matter: Influence of Capping Agent and Solution Conditions, *Langmuir*, 2015, **31**, 8865–8872.
16 J. Dobias and R. Bernier-Latmani, Silver Release from Silver Nanoparticles in Natural Waters, *Environ. Sci. Technol.*, 2013, **47**, 4140–4146.
17 L. Kvitek, A. Panacek, J. Soukupova, M. Kolar, R. Vecerova, R. Prucek, M. Holecova and R. Zboril, Effect of surfactants and polymers on stability and antibacterial activity of silver nanoparticles (NPs), *J. Phys. Chem. C*, 2008, **112**, 5825–5834.
18 K. Loza, J. Diendorf, C. Sengstock, L. Ruiz-Gonzalez, J. M. Gonzalez-Calbet, M. Vallet-Regi, M. Koller and M. Epple, The dissolution and biological effects of silver nanoparticles in biological media, *J. Mater. Chem. B*, 2014, **2**, 1634–1643.
19 D. M. Mitrano, J. F. Ranville, A. Bednar, K. Kazor, A. S. Hering and C. P. Higgins, Tracking dissolution of silver nanoparticles at environmentally relevant concentrations in laboratory, natural, and processed waters using single particle ICP-MS (spICP-MS), *Environ. Sci.: Nano*, 2014, **1**, 248–259.
20 M. Azodi, Y. Sultan and S. Ghoshal, Dissolution Behavior of Silver Nanoparticles and Formation of Secondary Silver Nanoparticles in Municipal Wastewater by Single-Particle ICP-MS, *Environ. Sci. Technol.*, 2016, **50**, 13318–13327.
21 F. Yi, G. Chen, G. Zeng, Z. Guo, W. Liu, Z. Huang, K. He and L. Hu, Influence of cysteine and bovine serum albumin on silver nanoparticle stability, dissolution, and toxicity to Phanerochaete chrysosporium, *RSC Adv.*, 2016, **6**, 106177–106185.
22 C. M. Park, J. Heo, N. Her, K. H. Chu, M. Jang and Y. Yoon, Modeling the effects of surfactant, hardness, and natural organic matter on deposition and mobility of silver nanoparticles in saturated porous media, *Water Res.*, 2016, **103**, 38–47.
23 S. R. Kanel, J. Flory, A. Meyerhoefer, J. L. Fraley, I. E. Sizemore and M. N. Goltz, Influence of natural organic matter on fate and transport of silver nanoparticles in

saturated porous media: laboratory experiments and modeling, *J. Nanopart. Res.*, 2015, **17**, 154.

24 X. Yang, S. Lin and M. R. Wiesner, Influence of natural organic matter on transport and retention of polymer coated silver nanoparticles in porous media, *J. Hazard. Mater.*, 2014, **264**, 161–168.

25 Y. Liang, S. A. Bradford, J. Simunek, H. Vereecken and E. Klumpp, Sensitivity of the transport and retention of stabilized silver nanoparticles to physicochemical factors, *Water Res.*, 2013, **47**, 2572–2582.

26 A. M. El Badawy, A. A. Hassan, K. G. Scheckel, M. T. Suidan and T. M. Tolaymat, Key factors controlling the transport of silver nanoparticles in porous media, *Environ. Sci. Technol.*, 2013, **47**, 4039–4045.

27 R. N. Lerner, Q. Lu, H. Zeng and Y. Liu, The effects of biofilm on the transport of stabilized zerovalent iron nanoparticles in saturated porous media, *Water Res.*, 2012, **46**, 975–985.

28 M. R. Mitzel and N. Tufenkji, Transport of industrial PVP-stabilized silver nanoparticles in saturated quartz sand coated with Pseudomonas aeruginosa PAO1 biofilm of variable age, *Environ. Sci. Technol.*, 2014, **48**, 2715–2723.

29 L. Lartigue, D. Alloyeau, J. Kolosnjaj-Tabi, Y. Javed, P. Guardia, A. Riedinger, C. Péchoux, T. Pellegrino, C. Wilhelm and F. Gazeau, Biodegradation of iron oxide nanocubes: high-resolution in situ monitoring, *ACS Nano*, 2013, **7**, 3939–3952.

30 G. S. Kiran, J. Selvin, A. Manilal and S. Sujith, Biosurfactants as green stabilizers for the biological synthesis of nanoparticles, *Crit. Rev. Biotechnol.*, 2011, **31**, 354–364.

31 A. A. Jimoh and J. Lin, Biosurfactant: A new frontier for greener technology and environmental sustainability, *Ecotoxicol. Environ. Saf.*, 2019, **184**, 109607.

32 D. K. Santos, R. D. Rufino, J. M. Luna, V. A. Santos and L. A. Sarubbo, Biosurfactants: Multifunctional Biomolecules of the 21st Century, *Int. J. Mol. Sci.*, 2016, **17**, 401.

33 R. M. Maier and G. Soberon-Chavez, Pseudomonas aeruginosa rhamnolipids: biosynthesis and potential applications, *Appl. Microbiol. Biotechnol.*, 2000, **54**, 625–633.

34 A. M. Abdel-Mawgoud, F. Lepine and E. Deziel, Rhamnolipids: diversity of structures, microbial origins and roles, *Appl. Microbiol. Biotechnol.*, 2010, **86**, 1323–1336.

35 H. F. Khalid, B. Tehseen, Y. Sarwar, S. Z. Hussain, W. S. Khan, Z. A. Raza, S. Z. Bajwa, A. G. Kanaras, I. Hussain and A. Rehman, Biosurfactant coated silver and iron oxide nanoparticles with enhanced anti-biofilm and anti-adhesive properties, *J. Hazard. Mater.*, 2019, **364**, 441–448.

36 W. Xue, D. Huang, G. Zeng, J. Wan, C. Zhang, R. Xu, M. Cheng and R. Deng, Nanoscale zero-valent iron coated with rhamnolipid as an effective stabilizer for immobilization of Cd and Pb in river sediments, *J. Hazard. Mater.*, 2018, **341**, 381–389.

37 M. Basnet, A. Gershanov, K. J. Wilkinson, S. Ghoshal and N. Tufenkji, Interaction between palladium-doped zerovalent iron nanoparticles and biofilm in granular porous media: characterization, transport and viability, *Environ. Sci.: Nano*, 2016, **3**, 127–137.

38 M. Basnet, C. Di Tommaso, S. Ghoshal and N. Tufenkji, Reduced transport potential of a palladium-doped zero valent iron nanoparticle in a water saturated loamy sand, *Water Res.*, 2015, **68**, 354–363.

39 M. Basnet, S. Ghoshal and N. Tufenkji, Rhamnolipid biosurfactant and soy protein act as effective stabilizers in the aggregation and transport of palladium-doped zerovalent iron nanoparticles in saturated porous media, *Environ. Sci. Technol.*, 2013, **47**, 13355–13364.

40 C. A. Marangon, V. C. A. Martins, M. H. Ling, C. C. Melo, A. M. G. Plepis, R. L. Meyer and M. Nitschke, Combination of Rhamnolipid and Chitosan in Nanoparticles Boosts Their Antimicrobial Efficacy, *ACS Appl. Mater. Interfaces*, 2020, **12**, 5488–5499.

41 J. P. Saikia, P. Bharali and B. K. Konwar, Possible protection of silver nanoparticles against salt by using rhamnolipid, *Colloids Surf., B*, 2013, **104**, 330–332.

42 C. B. B. Farias, A. F. Silva, R. D. Rufino, J. M. Luna, J. E. G. Souza and L. A. Sarubbo, Synthesis of silver nanoparticles using a biosurfactant produced in low-cost medium as stabilizing agent, *Electron. J. Biotechnol.*, 2014, **17**, 122–125.

43 S. Liao, A. Ghosh, M. D. Becker, L. M. Abriola, N. L. Cápiro, J. D. Fortner and K. D. Pennell, Effect of rhamnolipid biosurfactant on transport and retention of iron oxide nanoparticles in water-saturated quartz sand, *Environ. Sci.: Nano*, 2021, **8**, 311–327.

44 A. M. Mittelman, A. Taghavy, Y. Wang, L. M. Abriola and K. D. Pennell, Influence of dissolved oxygen on silver nanoparticle mobility and dissolution in water-saturated quartz sand, *J. Nanopart. Res.*, 2013, **15**, 330–332.

45 K.-M. Yao, M. T. Habibian and C. R. O'Melia, Water and waste water filtration. Concepts and applications, *Environ. Sci. Technol.*, 1971, **5**, 1105–1112.

46 Y. Wang, Y. Li, J. D. Fortner, J. B. Hughes, L. M. Abriola and K. D. Pennell, Transport and retention of nanoscale C60 aggregates in water-saturated porous media, *Environ. Sci. Technol.*, 2008, **42**, 3588–3594.

47 D. P. Cassidy, A. J. Hudak, D. D. Werkema, E. A. Atekwana, S. Rossbach, J. W. Duris, E. A. Atekwana and W. A. Sauck, In Situ Rhamnolipid Production at an Abandoned Petroleum Refinery, *Soil Sediment Contam.*, 2010, **11**, 769–787.

48 N. Toride, F. Leij and M. T. Van Genuchten, *The CXTFIT code for estimating transport parameters from laboratory or field tracer experiments, Version 2.1, Research Report No. 137*, Agricultural Research Service, US Department of Agriculture, Riverside, California, 1995.

49 M. V. Smoluchowski, Versuch einer mathematischen Theorie der Koagulationskinetik kolloider Lösungen, *Z. Phys. Chem.*, 1918, **92**, 129–168.

50 A. M. Mittelman, J. D. Fortner and K. D. Pennell, Effects of ultraviolet light on silver nanoparticle mobility and dissolution, *Environ. Sci.: Nano*, 2015, **2**, 683–691.

51 D. A. Armbruster and T. Pry, Limit of blank, limit of detection and limit of quantitation, *Clin. Biochem. Rev.*, 2008, **29**(Suppl 1), S49–S52.

52 Y. Li, Y. Wang, K. D. Pennell and L. M. Abriola, Investigation of the transport and deposition of fullerene (C60) nanoparticles in quartz sands under varying flow conditions, *Environ. Sci. Technol.*, 2008, **42**, 7174–7180.
53 N. Tufenkji and M. Elimelech, Correlation equation for predicting single-collector efficiency in physicochemical filtration in saturated porous media, *Environ. Sci. Technol.*, 2004, **38**, 529–536.
54 W. Zhang, Y. Yao, N. Sullivan and Y. Chen, Modeling the primary size effects of citrate-coated silver nanoparticles on their ion release kinetics, *Environ. Sci. Technol.*, 2011, **45**, 4422–4428.
55 S. T. Dubas and V. Pimpan, Humic acid assisted synthesis of silver nanoparticles and its application to herbicide detection, *Mater. Lett.*, 2008, **62**, 2661–2663.
56 L. R. Pokhrel, B. Dubey and P. R. Scheuerman, Impacts of select organic ligands on the colloidal stability, dissolution dynamics, and toxicity of silver nanoparticles, *Environ. Sci. Technol.*, 2013, **47**, 12877–12885.
57 A. R. Mendoza, J. M. Patalinghug, G. Canonigo and J. Yee, Screening of rhamnolipids from pseudomonas spp. and evaluation of its antimicrobial and antioxidant potential, *Bact. Emp.*, 2020, **3**, 46–51.
58 J. Liu, D. A. Sonshine, S. Shervani and R. H. Hurt, Controlled release of biologically active silver from nanosilver surfaces, *ACS Nano*, 2010, **4**, 6903–6913.
59 T. Phenrat, N. Saleh, K. Sirk, H.-J. Kim, R. D. Tilton and G. V. Lowry, Stabilization of aqueous nanoscale zerovalent iron dispersions by anionic polyelectrolytes: adsorbed anionic polyelectrolyte layer properties and their effect on aggregation and sedimentation, *J. Nanopart. Res.*, 2007, **10**, 795–814.
60 A. R. Petosa, D. P. Jaisi, I. R. Quevedo, M. Elimelech and N. Tufenkji, Aggregation and deposition of engineered nanomaterials in aquatic environments: role of physicochemical interactions, *Environ. Sci. Technol.*, 2010, **44**, 6532–6549.
61 S. A. Bradford, J. Simunek, M. Bettahar, M. T. van Genuchten and S. R. Yates, Significance of straining in colloid deposition: Evidence and implications, *Water Resour. Res.*, 2006, **42**, W12S15.
62 Y. Wang, Y. Li, J. Costanza, L. M. Abriola and K. D. Pennell, Enhanced mobility of fullerene (C60) nanoparticles in the presence of stabilizing agents, *Environ. Sci. Technol.*, 2012, **46**, 11761–11769.
63 W. Zhang, B. Xiao and T. Fang, Chemical transformation of silver nanoparticles in aquatic environments: Mechanism, morphology and toxicity, *Chemosphere*, 2018, **191**, 324–334.
64 S. Bhattacharjee and M. Elimelech, Surface element integration: A novel technique for evaluation of DLVO interaction between a particle and a flat plate, *J. Colloid Interface Sci.*, 1997, **193**, 273–285.
65 K. A. Guzman, M. P. Finnegan and J. F. Banfield, Influence of surface potential on aggregation and transport of titania nanoparticles, *Environ. Sci. Technol.*, 2006, **40**, 7688–7693.